Lesion Load of the Corticospinal Tract Predicts Motor Impairment in Chronic Stroke

Lin L. Zhu, Robert Lindenberg, Michael P. Alexander and Gottfried Schlaug

The online version of this article, along with updated information and services, is
located on the World Wide Web at:

http://stroke.ahajournals.org/cgi/content/full/41/5/910

Lesion Load of the Corticospinal Tract Predicts Motor Impairment in Chronic Stroke

Lin L. Zhu, BS; Robert Lindenberg, MD; Michael P. Alexander, MD; Gottfried Schlaug, MD, PhD

Background and Purpose—Previous studies have shown motor impairment after a stroke relates to lesion size and location, but unexplained variability in recovery still exists. In this study, we used lesion-mapping techniques in combination with diffusion tensor imaging to quantitatively test the hypothesis that motor recovery in patients with chronic stroke is inversely related to the proportion of the corticospinal tract (CST) affected by the lesion.

Methods—We studied 50 patients with chronic stroke, all of whom presented with moderate to severe motor impairments in the acute stage, using high-resolution anatomic MRI. We evaluated the degree of motor impairment with the Upper Extremity module of the Fugl-Meyer Assessment. To analyze the relationship between CST damage and impairment scores, we calculated a CST-lesion load for each patient by overlaying the patient's lesion map with a probabilistic tract derived from diffusion tensor images of age-matched healthy subjects.

Results—CST-lesion load was a significant predictor of motor deficit. Infarct size, despite correlating with motor scores, did not significantly predict impairment.

Conclusions—Our results show the degree of functional motor deficit after a stroke is highly dependent on the overlap of the lesion with the CST and not lesion size per se. In the future, automated calculation of CST-lesion load may allow more precise prediction of motor impairment after stroke. (*Stroke*. 2010;41:910-915.)

Key Words: corticospinal tract ■ diffusion tensor imaging ■ lesion mapping ■ motor recovery

Scientists have used many different neurophysiological and imaging techniques in their attempts to identify the major predictors of motor impairment in chronic stroke. Results of structural imaging studies have suggested that both lesion size[1,2] and lesion location[3–6] correlate with impairment and that the involvement of motor-related cortical regions (both primary and nonprimary motor areas), corona radiata, and internal capsule progressively decrease the probability of upper limb functional recovery.[3,6] These findings are complemented by results of recent diffusion tensor imaging (DTI) studies,[7] which established relationships between impairment in the acute and subacute phases and damage to the descending motor tracts.[8–11] Nevertheless, much of the variability in recovery remains unexplained due to the lack of advanced quantitative mapping tools that directly associate lesion location with relevant fiber tracts.

The ability to predict motor impairment based on lesion topography and measures of fiber tract damage can be enhanced by using lesion–behavior mapping techniques. When performed on a voxel-by-voxel basis, these methods are particularly advantageous because they can identify those brain regions critical for certain behaviors without a priori hypotheses.[12,13] For motor impairment in patients with chronic stroke, however, a priori hypotheses are appropriate because the functional role of the motor cortex and descending motor tracts has already been clearly demonstrated. As such, region of interest-based lesion analyses can be used to examine whether extent of damage to specific, predetermined fiber tracts can serve as a surrogate marker of impairment while at the same time avoiding the possible decrease in statistical power associated with voxel-by-voxel methods.[14] In addition, analyses combining lesion site and lesion size with fiber tract morphology have the potential to further our understanding of clinicoanatomic correlations and to delineate the fundamental processes that underlie motor recovery.

Accordingly, we overlaid lesion maps of 50 patients with stroke with a DTI-derived probabilistic map of the corticospinal tract (CST) and quantitatively examined the relationship between volume of lesion–CST overlap and motor impairment after stroke. We hypothesized that motor recovery is inversely related to the proportion of the CST affected by the lesion and, furthermore, that extent of lesion damage along the CST would be a better predictor of motor outcome than lesion size alone.

Methods

Subjects

The study group consisted of 50 patients, all of whom had ischemic strokes in the anterior circulation at least 6 months before entering

the study (12 women; mean age 58.6±13.9 years; median time poststroke 17.1 months, interquartile range 6.5 to 37.5 months; 21 right hemisphere and 29 left hemisphere strokes; 48 right-handed and 2 left-handed individuals). Each patient had a Medical Research Council strength grade ≤3/5 in the extensor muscles of the affected upper extremity in the first 24 hours after symptom onset. All patients in this study required inpatient rehabilitation, which consisted of standard physical and occupational therapy. Exclusion criteria were: bihemispheric or brain stem infarcts, primary intracerebral hemorrhages, history of stroke or consecutive stroke, or other concomitant neurological diseases. Patients were assessed using the Upper Extremity module of the Fugl-Meyer Assessment (UE-FM).[15] The UE-FM is a 30-item motor function assessment with scores ranging from 0 to 66; higher scores reflect more complete functional recovery. It is the most frequently used clinical motor impairment test in stroke rehabilitation research.[16]

An additional 10 healthy subjects were enrolled as age-matched control subjects (4 women; mean age 58.2±12.2 years); age at assessment for this study did not differ significantly between the patient group and the healthy control group (F[1,58]=0.006, *P*=0.940). All control subjects were right-handed and had no history of stroke or other neurological or psychiatric diseases. Routine MRI of their brains did not show any focal abnormalities and there was no evidence of clinically silent strokes. This study was approved by the local Institutional Review Board, and all participants gave written informed consent.

MRI Acquisition and Preprocessing

All participants were scanned on a 3-T GE scanner using a standard radiofrequency head coil. Head motion was minimized by foam padding and forehead-restraining straps. A T1-weighted high-resolution scan (voxel resolution: $0.93 \times 0.93 \times 1.5$ mm^3) and a set of axial fluid-attenuated inversion recovery images ($0.5 \times 0.5 \times 5$ mm^3) were acquired. T1-weighted and fluid-attenuated inversion recovery images were realigned and spatially normalized into images of isotropic voxel size ($2 \times 2 \times 2$ mm^3) using SPM5 (Wellcome Department of Neurology, London, UK) implemented in Matlab (The Mathworks Inc, Natick, Mass). For patients with extensive lesions, the infarct was excluded from the cost function calculation of the spatial normalization process[17] using lesion masks drawn in MRIcro.[18]

Lesion Mapping

We used MRIcro[18] to define the lesions in the spatially normalized T1-weighted images. For each patient, we manually outlined the lesion area on each slice of the normalized T1-weighted images while using the fluid-attenuated inversion recovery images as an additional guide to confirm the extent of the lesion. In cases with marked ventricular dilatation due to extensive ischemic lesions and consequent hemispheric atrophy, no part of the dilated ventricle was included in the lesion area. Lesions were drawn by a single rater who was blinded to the patients' UE-FM scores. A second blinded rater drew lesions in a subset of 10 patients to calculate an interobserver reliability (R^2=0.92). To display all lesions on the same side during final calculations, right hemispheric lesion maps (n=21) were mirrored across the midsagittal axis.

DTI: Image Acquisition and Analysis

The control subjects underwent DTI using a single-shot, spin-echo echoplanar image sequence with the following parameters: TR=10 seconds, TE=86.9 ms, resolution $2.6 \times 2.6 \times 2.6$ mm^3, 30 noncollinear diffusion directions with a *b* value of 1000 s/mm^2, and 6 acquisitions with a value of 0 s/mm^2. A total of 56 slices covered the entire brain, including the brain stem. Fractional anisotropy, a measure of the degree of directional preference of water diffusion, was calculated for each brain voxel.

Diffusion tensors were calculated for every voxel using MedINRIA 1.7,[19] which performs the estimation with least squares on the linearized version of the Stejskal and Tanner diffusion equation.[20] After estimation, nonpositive tensors were detected and replaced by the Log-Euclidian average of all positive–definite neighboring tensors. Log-Euclidian interpolation[21] has been shown to preserve tensor volume (ie, interpolation of tensor volume is monotonic) and, consequently, to not introduce more diffusion than there is initially (no swelling effect[22]).

Tractography was then applied to the DTI data to reconstruct white matter tracts by successively following the path of preferred direction of water diffusion. Fiber tracts were traced using tensor lines,[23] a modified streamline algorithm that connects adjacent voxels with similar principal eigenvectors while simultaneously using advection vectors to stabilize propagation through regions with nonlinear preferential diffusion. Trilinear Log-Euclidean interpolation[21] was used throughout tracking to produce fibers with smoother trajectories.

We applied a threshold fractional anisotropy value of 0.2 and a smoothness factor[23] of 0.2 for continuous fiber reconstruction; these parameters are similar to those reported by other researchers who have used continuous tracking algorithms to reconstruct fibers.[23,24]

Three regions of interest (ROIs) were drawn on each patient's fractional anisotropy images. The analysis was started with an ROI in the posterior limb of the internal capsule (at a level corresponding to z=8 of a spatially normalized brain in Talairach space[25]). A second ROI was drawn in the anterior pons (basis pontis; z=−24), where neuroanatomical[26] and tractography studies[27] locate the fiber bundle constituting the pyramidal tract. A logical *AND* function was added so that only fibers passing through both the posterior limb of the internal capsule and basis pontis were considered for further analysis. A third ROI included the precentral gyrus along with its underlying white matter (z=50). A logical *AND* function was also added for this ROI so that only those fibers originating in the precentral gyrus and passing through both the posterior limb of the internal capsule and the pons were designated as part of the CST. Fibers that went to the cerebellum were excluded by drawing ROIs in the superior cerebellar peduncle and the middle cerebellar peduncle and applying a logical *NOT* function in conjunction with the other ROIs.

The reconstructed fiber tract of each control subject was transformed into a binary image and spatially normalized using SPM5. We abstained from using patients' CSTs because their structurally abnormal tracts would have varied greatly due to the ischemic lesions and subsequent Wallerian degeneration.[28,29]

## Calculation of Lesion–CST Overlap

After normalization, the binary CSTs of the 10 healthy control subjects were summed to generate a fiber map using Matlab (Figure 1). Voxel intensities ranged from $I=0$ (ie, voxel is not part of the CST in any of the subjects) to $I=10$ (ie, voxel is part of the CST in all 10 subjects); thus, the probability that a particular voxel would be part of the CST was calculated as one tenth of the voxel's intensity.

For each lesion, a raw lesion–tract overlap volume (V_{raw}) was calculated by overlaying the lesion map onto the probabilistic CST and summing the intensities of all intersecting voxels. This calculation is denoted by the following equation:

$$V_{raw} = \sum_{n=1}^{n_{max}} \left[\frac{1}{10} \cdot I(n) \cdot (\text{voxel volume}) \right],$$

where n_{max} is the total number of intersecting voxels between the lesion map and fiber map and $I(n)$ is the intensity of the nth voxel (as represented in the fiber map). It should be noted that this method weighs voxels according to their individual probabilities of being part of the CST as opposed to treating all voxels with intensities above a certain threshold equally (ie, using isocontours[30,31]).

A weighted lesion–tract overlap volume was then calculated for each lesion using a method similar to the previously used proportional grid system.[3] This weighted overlap accounts for the narrowing of the CST as it descends from the motor cortex to the posterior limb of the internal capsule by multiplying the lesion–tract overlap on each slice by the ratio of the maximum cross-sectional area of the tract to the cross-sectional area of the tract on that particular slice.
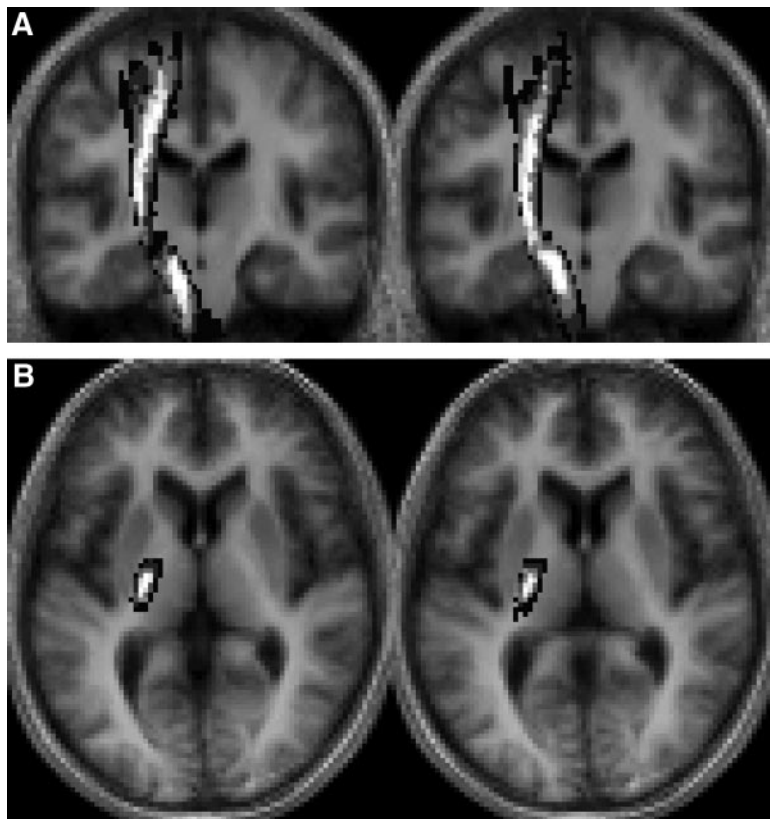
Figure 1. Probabilistic CST fiber map. A, The coronal slices shown correspond to y=−20 and −18 and (B) the axial slices correspond to z=6 and 4 in Talairach space.[25]

Although the proportional grid system—which used the Talairach and Tournoux atlas[25] as a reference—arbitrarily divided the region between the motor cortex and the intercommissural plane into 5 levels (1 cortical and 4 subcortical layers) and assigned a different weighting factor to each layer, we instead chose to calculate a different weighting factor for each individual slice (x) at every intensity level (I). For a particular slice x containing $m(x, I)$ voxels with intensity $\geq I$, a weighting factor $f(x, I)$ was calculated as:

$$f(x, I) = \frac{m(x^*, I)}{m(x, I)},$$

where $m(x^*, I)$ denotes the number of voxels on the slice x^* that contains the most voxels of intensity $\geq I$. Thus, for any intensity I, the slice (x^*) with the most voxels $\geq I$ was assigned a weighting factor of $f(x^*, I)=1$. For each patient, a weighted lesion–CST volume was then calculated using the following equation:

$$V_{weighted} = \sum_{n=1}^{n_{max}} \left[V_{raw} \cdot f(x(n), I(n)) \right]$$
$$= \sum_{n=1}^{n_{max}} \left[\frac{1}{10} \cdot I(n) \cdot (\text{voxel volume}) \cdot f(x(n), I(n)) \right],$$

where n_{max} is the total number of intersecting voxels between the lesion map and fiber map, $I(n)$ is the intensity of the nth voxel located on slice $x(n)$, and $f(x(n), I(n))$ is the weighting factor for the voxel. We will refer to the variables V_{raw} and $V_{weighted}$ as raw and weighted CST-lesion load, respectively.

Results

Motor impairment correlated significantly with raw CST-lesion load ($R^2=0.664$, $P<0.001$; Figure 2A), weighted CST-lesion load ($R^2=0.724$, $P<0.001$; Figure 2B), and lesion size ($R^2=0.307$, $P<0.001$; Figure 2C).

A regression analysis was first conducted using raw CST-lesion load and lesion size as predictors of motor impairment (adjusted $R^2=0.656$, $P<0.001$). Whereas raw CST-lesion load significantly predicted UE-FM scores (partial $R^2=0.524$, $P<0.001$), lesion size was shown not to be a significant predictor of motor impairment (partial $R^2=0.016$, $P=0.383$). A second regression analysis was then conducted using weighted CST-lesion load and lesion size as predictors of motor impairment (adjusted $R^2=0.720$, $P<0.001$). Again, lesion size did not significantly predict motor impairment (partial $R^2=0.023$, $P=0.302$), whereas the weighted CST-lesion load did (partial $R^2=0.613$, $P<0.001$).

A final regression analysis was conducted using lesion size and both raw and weighted CST-lesion load as predictors of UE-FM score (adjusted $R^2=0.727$, $P<0.001$). Weighted CST-lesion load was shown to be a better predictor (partial $R^2=0.223$, $P=0.001$) than either raw CST-lesion load (partial $R^2=0.045$, $P=0.147$) or lesion size (partial $R^2=0.007$, $P=0.568$).

Discussion

We used lesion–behavior mapping techniques to analyze the relationship between motor function and lesion load of the CST in patients with chronic stroke. Our results inform a longstanding debate regarding the relationship between infarct size and clinical outcome measures of stroke. Although several studies have reported significant but moderate correlations between motor impairment and lesion size, others have argued that no statistically significant relationship exists.[32] In our study, infarct size, despite correlating with
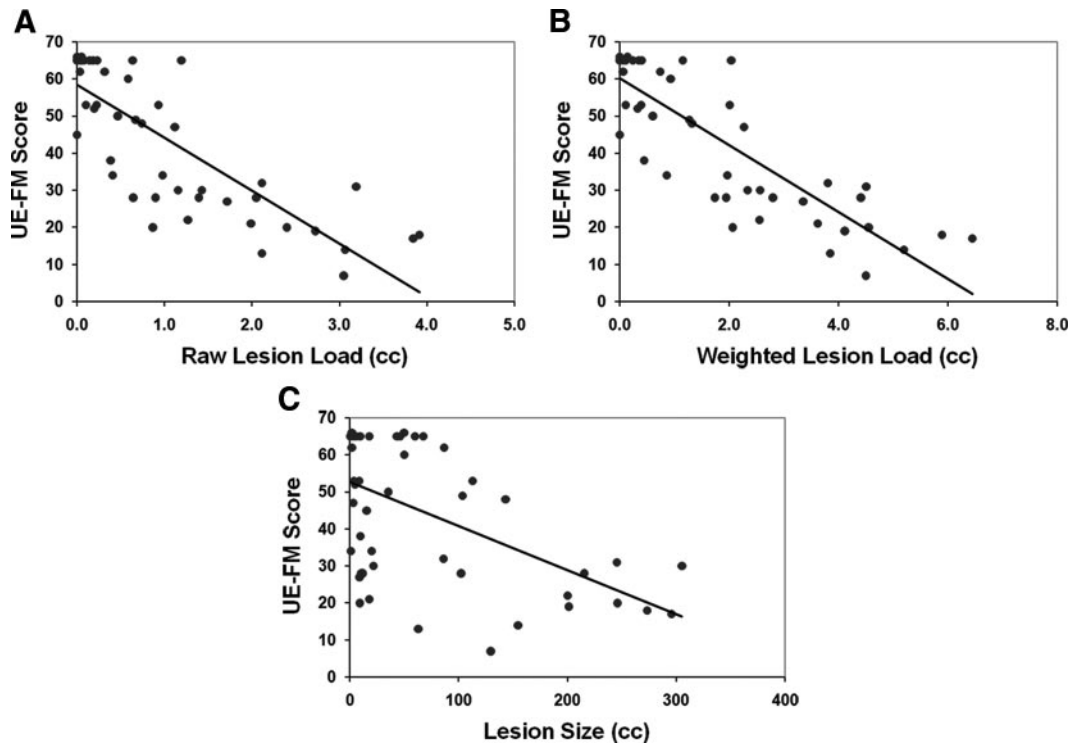
Figure 2. Regression analyses. UE-FM scores are plotted as functions of (A) raw CST-lesion load, (B) weighted CST-lesion load, and (C) lesion size.

UE-FM score, did not predict motor impairment. In contrast, the partial correlations of CST-lesion load with UE-FM scores remained highly significant in the regression analyses, which suggest that, in fact, infarct size is merely masking the effect of lesion damage within the CST (Figure 3).
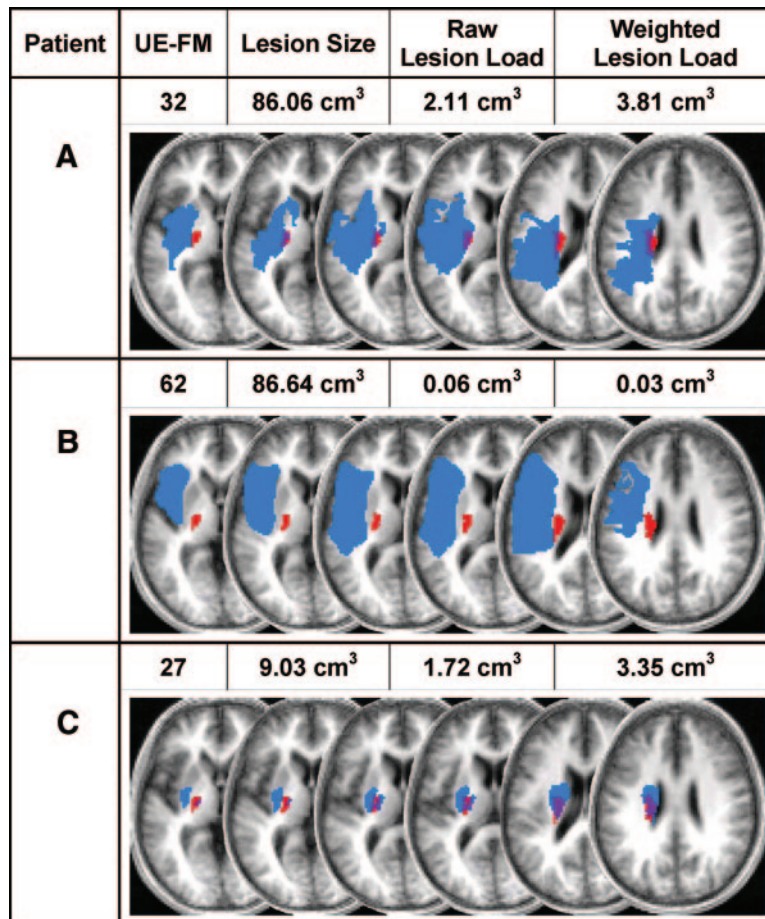
The highly significant linear correlation demonstrated between raw CST-lesion load and UE-FM score is in accordance with previous studies that have quantitatively examined the relationship between CST involvement within the ischemic lesion and motor outcome.[30,33,34] One such study analyzed infarct size with respect to CST involvement by overlaying a hand-drawn mask of descending motor tracts onto T2-weighted MR images.[34] The greatest proportional intersection of lesion with this mask on any single slice was found to be more highly correlated with motor impairment than lesion size; however, this maximum ratio of lesion to mask cross-sectional area was not found to be a significantly superior predictor of motor impairment as compared with infarct size, which the authors attributed to their rather small patient sample (n=18). Two studies that used variations of this approach resulted in comparable findings. In the first study,[33] the slices of greatest proportional overlap were determined by overlaying lesion maps of 3 patients with motor tracts derived from diffusion tensor images of healthy subjects; disconnections of the tracts were associated with differing hand-grip responses displayed by the patients. In another study,[30] lesion maps of 18 patients with mild to moderate impairments of the lower limb were overlaid onto a probabilistic fiber map derived from diffusion tensor images of 8 healthy, nonage-matched control subjects. Although gait parameters showed trends for correlation with both maximal

cross-sectional overlap as well as total lesion overlap, in contrast to our study, none of the correlations reached statistical significance. Our study complements these investigations by overlaying lesion maps from a large sample of patients with stroke onto a probabilistic, nonisocontour CST map derived from age-matched control subjects.

Our approach further expounds on the relationship between CST-lesion overlap and impairment by accounting for the narrowing of the CST as it descends from the precentral gyrus. We applied slicewise weighting factors to our probabilistic fiber map similar to those utilized in the previously used proportional grid system[3] and, as such, were able to more realistically model the anatomic topography of the CST. Consequently, the weighted CST-lesion load, which quantifies motor impairment in terms of tract geometry, was shown to be an even better predictor of motor impairment than the raw overlap variable.

Future longitudinal studies may wish to use CST-lesion load measured in the acute phase to examine the relationship between CST involvement and subsequent motor impairment. One study showed integrity of the CST—as classified using acute-phase DTI scans—to predict motor outcome at 6 months in patients with pontine infarcts[9]; whether or not a similar causal relationship exists between acute/subacute lesion–tract overlap in hemispheric strokes and motor outcome in the chronic phase has not yet been determined.

Our study is not without its limitations; we have generated our probabilistic CST map using fibers that were tracked using a modified streamline algorithm. Although this single-fiber method has been shown to be able to traverse regions of oblate tensors and, thus, reconstruct some crossing fibers,

Patient	UE-FM	Lesion Size	Raw Lesion Load	Weighted Lesion Load
A	32	86.06 cm³	2.11 cm³	3.81 cm³
B	62	86.64 cm³	0.06 cm³	0.03 cm³
C	27	9.03 cm³	1.72 cm³	3.35 cm³

Figure 3. CST-lesion load versus lesion size. Shown here are examples of 3 patients' motor impairment scores, lesion sizes, and lesion load volumes as well as their individual lesion maps (depicted in blue) overlaid onto the probabilistic fiber map (depicted in red). Overlap between lesion and CST is displayed in purple. The axial slices depicted correspond to z=0, 4, 8, 10, 20, and 28 in Talairach space.[25] Comparison of Patients A and B shows how 2 similarly sized lesions can produce markedly different CST-lesion loads and, accordingly, result in very different levels of motor impairment. Similarly, comparison of Patients A and C shows how 2 patients can display comparable CST-lesion loads and functional ability despite drastically different overall lesion volumes.

future studies may wish to use other tractography methods that might be better suited for fiber reconstruction in regions of complex crossings (eg, multitensor or q-ball analysis). Multifiber probabilistic models may be particularly useful for researchers examining motor functions represented more laterally on the cortex or behaviors served by nondominant fiber pathways.[35] Finally, by including the entire precentral gyrus as a cortical ROI, we have inevitably also tracked corticospinal fibers originating from the premotor cortex. Nevertheless, our approach, which is consistent with methods used in previous DTI studies,[10,36–38] is reliable and easily reproduced because the precentral gyrus can be easily identified. In contrast, no clear macroanatomic landmarks indicate the border between the primary motor and premotor cortices.

In conclusion, we have shown CST-lesion load—a new variable that combines lesion size and CST involvement into a single quantitative measure—to be a statistically significant predictor of motor impairment in patients with chronic stroke. The value of this new variable can be enhanced by using weighting factors to account for the narrowing of the CST as it descends from the precentral gyrus. The superiority of CST-lesion load as a predictor of motor deficit reinforces the notion that infarct localization and fiber tract integrity play critical roles in functional impairment. Our method, which complements established lesion mapping and DTI techniques, could be automated in the future to assist clinicians and researchers in making accurate prognoses of motor impairment after stroke.

Disclosures

None.

References

1. Mohr JP, Foulkes MA, Polis AT, Hier DB, Kase CS, Price TR, Tatemichi TK, Wolf PA. Infarct topography and hemiparesis profiles with cerebral convexity infarction: the Stroke Data Bank. *J Neurol Neurosurg Psychiatry*. 1993;56:344–351.
2. Saver JL, Johnston KC, Homer D, Wityk R, Koroshetz W, Truskowski LL, Haley EC. Infarct volume as a surrogate or auxiliary outcome measure in ischemic stroke clinical trials. The RANTTAS Investigators. *Stroke*. 1999;30:293–298.
3. Binkofski F, Seitz RJ, Arnold S, Classen J, Benecke R, Freund HJ. Thalamic metabolism and corticospinal tract integrity determine motor recovery in stroke. *Ann Neurol*. 1996;39:460–470.
4. Crafton KR, Mark AN, Cramer SC. Improved understanding of cortical injury by incorporating measures of functional anatomy. *Brain*. 2003; 126:1650–1659.
5. Schiemanck SK, Kwakkel G, Post MW, Kappelle LJ, Prevo AJ. Impact of internal capsule lesions on outcome of motor hand function at one year post-stroke. *J Rehabil Med*. 2008;40:96–101.
6. Shelton FN, Reding MJ. Effect of lesion location on upper limb motor recovery after stroke. *Stroke*. 2001;32:107–112.

7. Ciccarelli O, Catani M, Johansen-Berg H, Clark C, Thompson A. Diffusion-based tractography in neurological disorders: concepts, applications, and future developments. *Lancet Neurol*. 2008;7:715–727.

8. Cho SH, Kim DG, Kim DS, Kim YH, Lee CH, Jang SH. Motor outcome according to the integrity of the corticospinal tract determined by diffusion tensor tractography in the early stage of corona radiata infarct. *Neurosci Lett*. 2007;426:123–127.

9. Jang SH, Bai D, Son SM, Lee J, Kim DS, Sakong J, Kim DG, Yang DS. Motor outcome prediction using diffusion tensor tractography in pontine infarct. *Ann Neurol*. 2008;64:460–465.

10. Konishi J, Yamada K, Kizu O, Ito H, Sugimura K, Yoshikawa K, Nakagawa M, Nishimura T. MR tractography for the evaluation of functional recovery from lenticulostriate infarcts. *Neurology*. 2005;64: 108–113.

11. Lee JS, Han MK, Kim SH, Kwon OK, Kim JH. Fiber tracking by diffusion tensor imaging in corticospinal tract stroke: topographical correlation with clinical symptoms. *Neuroimage*. 2005;26:771–776.

12. Bates E, Wilson SM, Saygin AP, Dick F, Sereno MI, Knight RT, Dronkers NF. Voxel-based lesion-symptom mapping. *Nat Neurosci*. 2003;6:448–450.

13. Karnath HO, Fruhmann Berger M, Kuker W, Rorden C. The anatomy of spatial neglect based on voxelwise statistical analysis: a study of 140 patients. *Cereb Cortex*. 2004;14:1164–1172.

14. Rorden C, Fridriksson J, Karnath H-O. An evaluation of traditional and novel tools for lesion behavior mapping. *Neuroimage*. 2009;44: 1355–1362.

15. Fugl-Meyer AR, Jaasko L, Leyman I, Olsson S, Steglind S. The post-stroke hemiplegic patient. 1. A method for evaluation of physical performance. *Scand J Rehabil Med*. 1975;7:13–31.

16. van Wijck FM, Pandyan AD, Johnson GR, Barnes MP. Assessing motor deficits in neurological rehabilitation: patterns of instrument usage. *Neurorehabil Neural Repair*. 2001;15:23–30.

17. Brett M, Leff AP, Rorden C, Ashburner J. Spatial normalization of brain images with focal lesions using cost function masking. *Neuroimage*. 2001;14:486–500.

18. Rorden C, Brett M. Stereotaxic display of brain lesions. *Behav Neurol*. 2000;12:191–200.

19. Toussaint N, Souplet JC, Fillard P. MedINRIA: Medical Image Navigation and Research Tool by INRIA. MICCAI '07 Workshop on Interaction in Medical Image Analysis and Visualization; Brisbane, Australia; 2007.

20. Basser PJ, Mattiello J, LeBihan D. MR diffusion tensor spectroscopy and imaging. *Biophys J*. 1994;66:259–267.

21. Fillard P, Pennec X, Arsigny V, Ayache N. Clinical DT-MRI estimation, smoothing, and fiber tracking with log-Euclidean metrics. *IEEE Trans Med Imaging*. 2007;26:1472–1482.

22. Arsigny V, Fillard P, Pennec X, Ayache N. Log-Euclidean metrics for fast and simple calculus on diffusion tensors. *Magn Reson Med*. 2006; 56:411–421.

23. Weinstein DM, Kindlmann GL, Lundberg EC. Tensorlines: advection–diffusion based propagation through diffusion tensor fields. 10th IEEE Visualization Conference. Washington, DC: IEEE Computer Society; 1999:249–254.

24. Schaechter JD, Perdue KL, Wang R. Structural damage to the corticospinal tract correlates with bilateral sensorimotor cortex reorganization in stroke patients. *Neuroimage*. 2008;39:1370–1382.

25. Talariach J, Tournoux P. *Co-planar Stereotaxic Atlas of the Human Brain*. New York: Thieme Medical Publishers; 1988.

26. Nieuwenhuys R, Voogd J, Huijzen CV. *The Human Central Nervous System,* IV ed. Berlin: Springer; 2008.

27. Wakana S, Jiang H, Nagae-Poetscher LM, van Zijl PC, Mori S. Fiber tract-based atlas of human white matter anatomy. *Radiology*. 2004;230: 77–87.

28. Lindberg PG, Skejø PH, Rounis E, Nagy Z, Schmitz C, Wernegren H, Bring A, Engardt M, Forssberg H, Borg J. Wallerian degeneration of the corticofugal tracts in chronic stroke: a pilot study relating diffusion tensor imaging, transcranial magnetic stimulation, and hand function. *Neurorehabil Neural Repair*. 2007;21:551–560.

29. Werring DJ, Toosy AT, Clark CA, Parker GJ, Barker GJ, Miller DH, Thompson AJ. Diffusion tensor imaging can detect and quantify corticospinal tract degeneration after stroke. *J Neurol Neurosurg Psychiatry*. 2000;69:269–272.

30. Dawes H, Enzinger C, Johansen-Berg H, Bogdanovic M, Guy C, Collett J, Izadi H, Stagg C, Wade D, Matthews PM. Walking performance and its recovery in chronic stroke in relation to extent of lesion overlap with the descending motor tract. *Exp Brain Res*. 2008;186:325–333.

31. Karnath HO, Rorden C, Ticini LF. Damage to white matter fiber tracts in acute spatial neglect. *Cereb Cortex*. 2009;19:2331–2337.

32. Mark VW, Taub E, Perkins C, Gauthier L, Uswatte G. MRI infarction load and CI therapy outcomes for chronic post-stroke hemiparesis. *Restor Neurol Neurosci*. 2008;26:13–33.

33. Newton JM, Ward NS, Parker GJ, Deichmann R, Alexander DC, Friston KJ, Frackowiak RS. Non-invasive mapping of corticofugal fibres from multiple motor areas—relevance to stroke recovery. *Brain*. 2006;129: 1844–1858.

34. Pineiro R, Pendlebury ST, Smith S, Flitney D, Blamire AM, Styles P, Matthews PM. Relating MRI changes to motor deficit after ischemic stroke by segmentation of functional motor pathways. *Stroke*. 2000;31: 672–679.

35. Behrens TE, Berg HJ, Jbabdi S, Rushworth MF, Woolrich MW. Probabilistic diffusion tractography with multiple fibre orientations: what can we gain? *Neuroimage*. 2007;34:144–155.

36. Kunimatsu A, Aoki S, Masutani Y, Abe O, Mori H, Ohtomo K. Three-dimensional white matter tractography by diffusion tensor imaging in ischaemic stroke involving the corticospinal tract. *Neuroradiology*. 2003; 45:532–535.

37. Lehericy S, Ducros M, Krainik A, Francois C, Van de Moortele PF, Ugurbil K, Kim DS. 3-D diffusion tensor axonal tracking shows distinct SMA and pre-SMA projections to the human striatum. *Cereb Cortex*. 2004;14:1302–1309.

38. Thomas B, Eyssen M, Peeters R, Molenaers G, Van Hecke P, De Cock P, Sunaert S. Quantitative diffusion tensor imaging in cerebral palsy due to periventricular white matter injury. *Brain*. 2005;128:2562–2577.